VNU Journal of Science: Mathematics – Physics, Vol. 35, No. 4(2019) 33-40

VNU Journal of Science: Mathematics - Physics

Journal homepage: https://js.vnu.edu.vn/MaP

Original Article

Synthesis and Characterization of Ni^{2+}-doped SnO_2 Powders

Trinh Thi Loan*, Nguyen Ngoc Long

Faculty of Physics, VNU University of Science, 334 Nguyen Trai, Hanoi, Vietnam

Received 03 June 2019
Revised 21 June 2019; Accepted 25 June 2019

Abstract: In this study, SnO_2:Ni^{2+} powders with dopant contents ranging from 0.0 to 12 mol% were synthesized by sol-gel method. The samples were characterized by X-ray diffraction (XRD) Raman spectroscopy, energy-dispersive X-ray spectrometer (EDS) and photoluminescense (PL) spectra. The XRD analysis shows that the samples doped with low Ni- concentrations exhibited single SnO_2crystalline phase, whereas the samples doped with high Ni- concentrations exhibited a mixture of SnO_2 and NiO phases. The lattice parameters of the SnO_2 host were independent of Ni^{2+} dopant content, while Raman mode positions were dependent on Ni^{2+} dopant content. The PL spectrum of the undoped SnO_2 was characterized by the emission peaks due to near band edge (NBE) emission and the violet emission peaks associated with surface dangling bonds or oxygen vacancies and Sn interstitials.

Keywords: SnO_2:Ni^{2+} powders, sol-gel method, photoluminescense

1. Introduction

Tin dioxide, SnO_2, is an important n-type semiconductor material, having a wide band gap (E_g = 3.62 eV, at 300 K for bulk). It is well-known in potential applications such as gas sensors [1], dye-sinsitized solar cells (DSSCs) [2], transparent conducting electrodes [3] and catalyst supports [4]. There are many methods for synthesis of SnO_2 materials, for instance photochemical growth at the air–water interface, thermal decomposition, sol-gel, surfactant-assisted solvothermal, hydrothermal synthesis and sono-chemical method [5]. It is seen that metal cations doped SnO_2 nanomaterials proved to be a successful tool for tailoring their electrical, optical, and microstructural properties [5].

*Corresponding author.
Email address: loan.trinhthi@gmail.com

https//doi.org/ 10.25073/2588-1124/vnumap.4356

In this work, we present the investigation results on the structure characteristics and photoluminescence properties of Ni^{2+}-doped SnO_2 powders that were prepared by sol-gel method.

2. Experimental

The SnO_2 powders doped with different amounts of Ni^{2+} ions were synthesized by sol-gel method using $C_2H_4(OH)_2$ aqueous solution, $SnCl_2.2H_2O$ salts and $Ni(NO_3)_2$ aqueous solution as the precursors. First, 2.3 g of $SnCl_2.2H_2O$ salts was dissolved in 30 ml of solution of $C_2H_4(OH)_2$ by stirring. Then, the proper amount of 0.02 M of solution of $Ni(NO_3)_2$ was added to the above solution. With such initial chemicals, a suggested composition of the same could be of $Sn_{1-x}Ni_xO_2$ with x ranging from 0 to 0.12. The last mixed solution was kept at constant temperature of 150 ^oC, with rigorous stirring until a highly viscous gel was formed. After drying at 220 ^oC for 24 h the gel was annealed at 1000 ^oC in air for 3h.

The crystalline structure of Ni^{2+}-doped SnO_2 was checked by XRD on a Siemens D5005 Bruker, Germany X-ray diffractometer (XRD), using Cu-Kα1 irradiation (λ = 1.54056 Å). Raman spectra were measured on LabRam HR800, Horiba spectrometer with 632.8 nm excitation. The composition of the samples was determined by an energy-dispersive X-ray spectrometer (EDS) Oxford Isis 300 attached to the JEOL-JSM 540 LV scanning electron microscope. The photoluminescence (PL) spectra were measured at room temperature using a Fluorolog FL3-22 Jobin Yvon Spex, USA spectrofluorometer with a xenon lamp of 450 W being used as an excitation source.

3. Results and discussion

3.1. Structure characterization

The XRD patterns of the SnO_2:Ni^{2+} samples with different doping concentration are shown in Fig.1. It is clearly seen that the synthesized samples with doping concentrations 0.0 mol%,1.0 mol%, 3.0 mol% and 6.0 mol% exhibit single SnO_2 crystalline phase. In each pattern, the eleven diffraction peaks are observed at around 2θ angles: 26.6^o, 33.9^o, 38.0^o, 39.0^o, 42.7^o, 51.9^o, 54.8^o, 57.8^o, 61.9^o, 64.8^o and 66.0^o, which are assigned to the diffraction peaks from the (110), (101), (200), (111), (210), (211), (220), (002), (310), (112) and (301) planes of SnO_2 with tetragonal rutile structure, respectively (JCPDS card: 21-1250). No characteristic peaks of the impurity phase have been observed (lines a, b, c and d in Fig.1A). The lattice parameters of the SnO_2 sample undoped calculated from the XRD patterns are a = b = 4.734 ± 0.002 Å and c = 3.183 ± 0.002 Å, which are in good agreement with the standard values (a = b = 4.73800 Å và c = 3.18800 Å (JCPDS card: 21-1250)). However, for the sample with doping concentrationof 9.0 mol%, beside the diffraction peaks of the SnO_2 phase, some weak new peaks at 2θ angles 37.3^o, 43.3^o and 62.9^o of the NiO phase are also observed (line e in Fig.1B). These new peaks become stronger in XRD patterns of the sample containing 12.0 mol% Ni^{2+} (line f in Fig.1B).

The lattice parameters of the samples calculated from the XRD patterns for a tetragonal lattice were calculated by formula:

$$d_{hkl} = \frac{a}{\sqrt{h^2 + k^2 + (c/a)^2 l^2}} \quad (1)$$

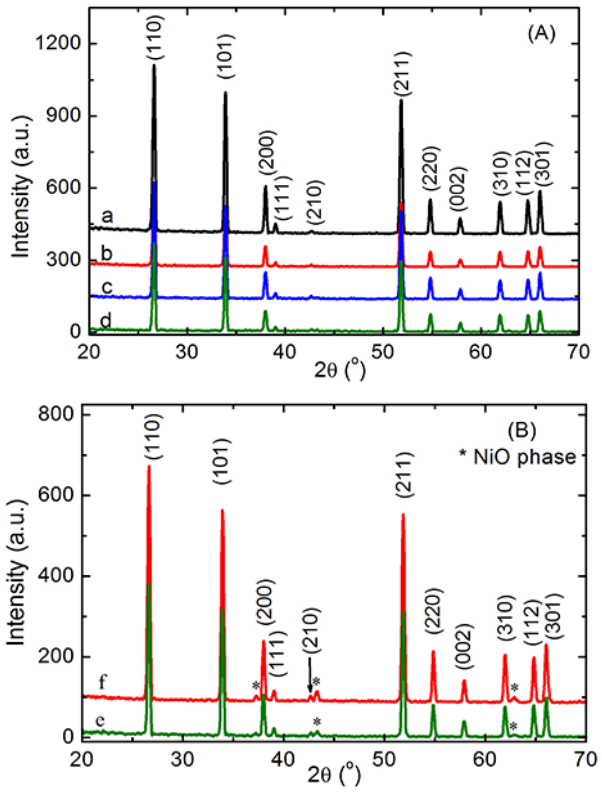

Fig.1. XRD patterns of the Ni^{2+}-doped SnO_2 samples with different doping concentration: (A): a- 0.0 mol%, b- 1.0 mol%, c- 3.0 mol% and d- 6.0 mol%; (B): e- 9.0 mol% and f- 12.0 mol%.

The results of the calculation for *a* and *c*, using data of d_{hkl} in XRD, are shown in Table 1. The lattice parameters of the samples doped with lower 9 mol%- Ni concentrations remain no change, independent on Ni^{2+} content. This is because the effective ionic radii of Ni^{2+} ion and Sn^{4+} ion in octahedral coordination are the same (0.69 Å).

Table 1. The lattice parameters of the SnO_2:Ni^{2+}samples with different doping concentration

Ni^{2+}content (mol%)	d_{110} (Å)	d_{101} (Å)	d_{211} (Å)	a = b (Å)	c (Å)
0.0	3.345	2.641	1.762	4.731 ± 0.001	3.183 ± 0.001
1.0	3.345	2.641	1.763	4.732 ± 0.002	3.184 ± 0.003
3.0	3.348	2.642	1.762	4.734 ± 0.002	3.183 ± 0.002
6.0	3.346	2.641	1.762	4.732 ± 0.001	3.183 ± 0.001

Raman scattering spectroscopy was employed to study the vibrational properties of the SnO_2:Ni^{2+} samples. It is well known that, SnO_2 has a tetragonal rutile crystalline structure with point group $D^{4h}{}_{14}$ and space group $P4_2$ /mnm. The unit cell consists of two metal atoms and four oxygen atoms. Each metal atom is situated amidst six oxygen atoms which approximately form the corners of a regular octahedron. Oxygen atoms are surrounded by three tin atoms which approximate the corners of an equilateral triangle. The 6 unit cell atoms give a total of 18 branches for the vibrational modes in the first Brillouin zone. Of these 18 modes, 4 are Raman active (three nondegenerated modes, A_{1g}, B_{1g},

B_{2g}, and a doubly degenerate E_g) [6]. The nondegenerate mode, A_{1g}, B_{1g}, and B_{2g}, vibrate in the plane perpendicular to the c axis while the doubly degenerated E_g mode vibrates in the direction of the c axis [6].

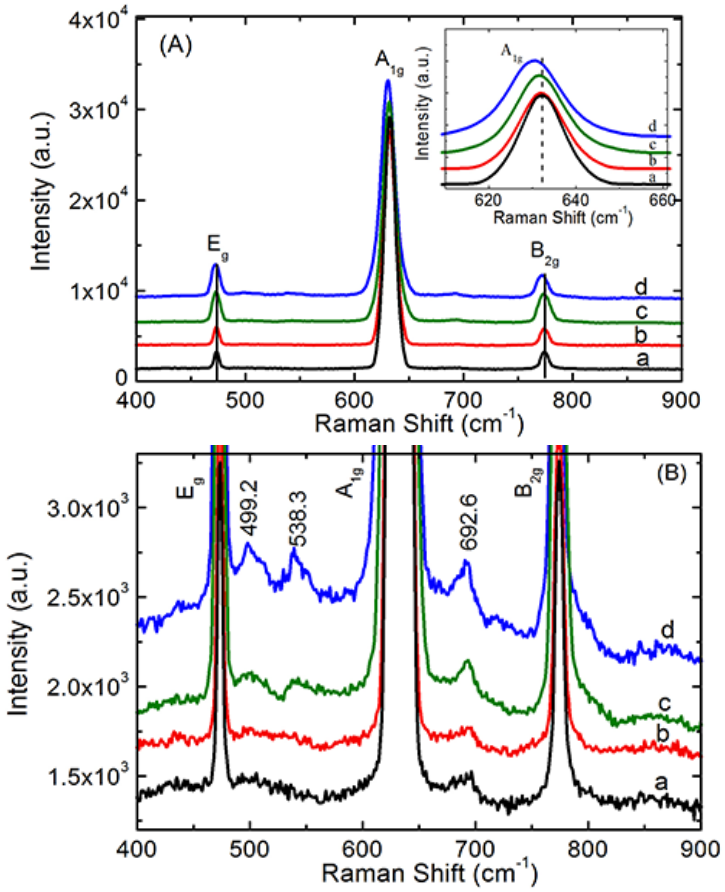

Fig. 2. Raman spectra of the Ni^{2+}-doped SnO_2 samples with different doping concentration: (A): a- 0 mol%, b- 1.0 mol%, c- 6.0 mol% and 12.0 mol%. (B): the zoom in of (A).

Fig.2 shows the Raman scattering spectrum of the Ni^{2+}-doped SnO_2 samples with doping concentrations: 0 mol%, 1.0 mol%, 6.0 mol% and 12.0 mol%. It can be confirmed from these Raman spectra that SnO_2 possess the characteristics of the tetragonal rutile structure, which are in accordance with the XRD results. It can be seen that Raman spectrum of Ni^{2+}-doped sample with low concentration of 1.0 mol% is quite similar to that of undoped SnO_2. In the Raman spectrum, the four Raman peaks at 473.4 cm^{-1}, 632.1 cm^{-1}, 692.6 cm^{-1} and 774.1 cm^{-1} were observed. The 473.4 cm^{-1} peak can be corresponding to E_g mode, which is related to the vibration of oxygen in the oxygen plan [7-9]. The 632.1 cm^{-1} and 774.1 cm^{-1} peaks can be corresponding to A_{1g} and B_{2g} vibration modes respectively, which are induced by the expansion and contraction vibration mode of Sn – O bonds and usually appear in bulk single crystals or polycrystalline SnO_2 materials [7-9]. The 692.6 cm^{-1} peak (noted by DA1 peak) can be assigned to space symmetry of the SnO_2 grain assemblage relating to existence of vacant lattice sites and local lattice disorder [7]. When the Ni^{2+} dopant concentration increases to 6.0 mol%, the Raman spectrum shows two weak new peaks at 499.2 and 538.3 cm^{-1}, which were not detected in bulk SnO_2. These new peaks become stronger in Raman spectrum of the

sample with 12.0 mol% Ni^{2+}. The weak Raman peaks at 499.2 cm^{-1} and 538.3 cm^{-1} were also observed in the work of Lu et al. [10]. They proposed that the weak Raman peak at 497 cm^{-1} might correspond to the IR-active modes of transverse optical phonons (TO) of A_{2u} modes [10,11], while appearance of the peak at 538.3 cm^{-1}(noted by DA2 peak) was a consequence of the disorder activation [10]. The reasons for the appearance of these "Raman-forbidden" modes could be manifold. Another possible reason might be that the oxygen vacancies induced the Raman activity [10]. The increase in oxygen vacancies maybe results from the assumed substitution of Sn^{4+} ions with Ni^{2+} cations of lower valences.

The frequency of Raman modes of the SnO_2 powders doped with different Ni^{2+} contents is shown Table 2. It is found that the frequency of Raman modes of the SnO_2 powders small changed and dependent on Ni^{2+} content. Although the effective ionic radius of Ni^{2+} ion and Sn^{4+} in octahedral coordination is the same, however the valency of Ni^{2+} and Sn^{4+} ions is different. Therefore, the incorporation of Ni^{2+} does not change the lattice parameters of SnO_2, but the Ni^{2+} dopants can cause the crystal distortions of the co-ordination around Ni in general, and the change of the symmetry of local crystal structure around Ni^{2+}. This can lead to the change of the strength of the Sn – O bonds, and thus the shift of the Raman modes.

Table 2. The frequency of Raman modes of the SnO_2 powders doped with different Ni^{2+} contents.

Ni^{2+} content (mol%)	TO of A_{2u} (cm^{-1})	DA2 (cm^{-1})	E_g (cm^{-1})	A_{1g} (cm^{-1})	DA1 (cm^{-1})	B_{2g} (cm^{-1})
0	-	-	473.4	632.1	693.2	774.1
1.0	-	-	473.4	632.1	694.9	774.1
6.0	500.7	538.3	472.9	631.6	692.3	773.4
12.0	499.2	538.1	472.3	630.5	692.6	771.9

The EDS spectra of the SnO_2 samples doped with 6.0 and 12.0 mol% Ni^{2+} are presented in Fig. 3. The EDS spectra exhibit the peaks related to the Sn, O and Ni elements, in addition, the characteristic peaks for Ni element increase in intensity when Ni^{2+} concentration increases. The results of the EDS analysis indicate that the Ni^{2+} ions are incorporated in Ti^{4+} lattice sites.

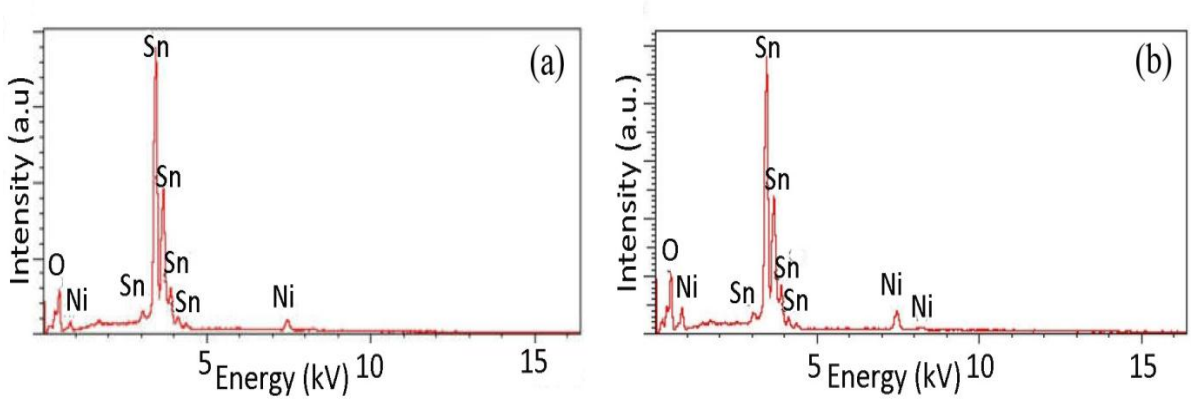

Fig. 3. The EDS spectra of the Ni^{2+}-doped SnO_2 samples with different doping concentrations: (a) 6.0 mol%, (b) 12.0 mol%.

3.2. Optical characterization

Fig. 4 shows the PL spectra of the undoped SnO_2 measured at room temperature. The excitation wavelength was 300 nm. It can be seen that the PL spectrum of the undoped SnO_2 is characterized by one prominent broad band peaking at 365 nm with some right shoulders at 395 nm, 412 nm, 438 nm, 452 nm, and 467 nm. It is well known that SnO_2 is a direct bandgap semiconductor, however, limited by its dipole-forbidden nature, the bandgap emission with the photon energy of 3.6 eV (344 nm) is prohibited at room temperature due to the selection rule [12]. Therefore, the intense peak at 365 nm and 395 nm are perhaps due to near band edge (NBE) emission [13-15]. The three shoulders/peaks at 412 nm, 438 nm, 452 nm are the violet emission associated with surface dangling bonds or oxygen vacancies and Sn interstitials [14]. The peak at 465 nm is due to doubly ionized oxygen vacancies [14].

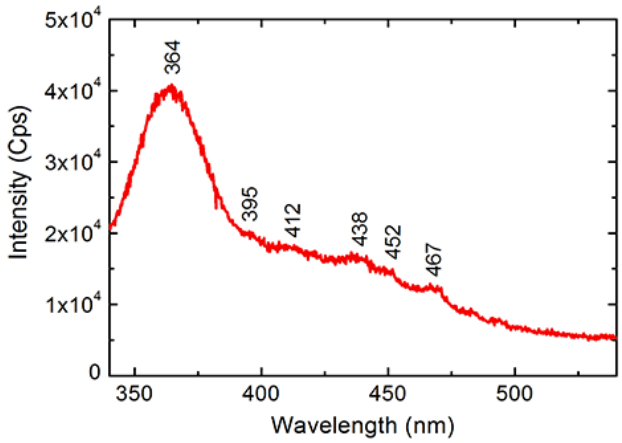

Fig. 4. PL spectra of undoped SnO_2 powder.

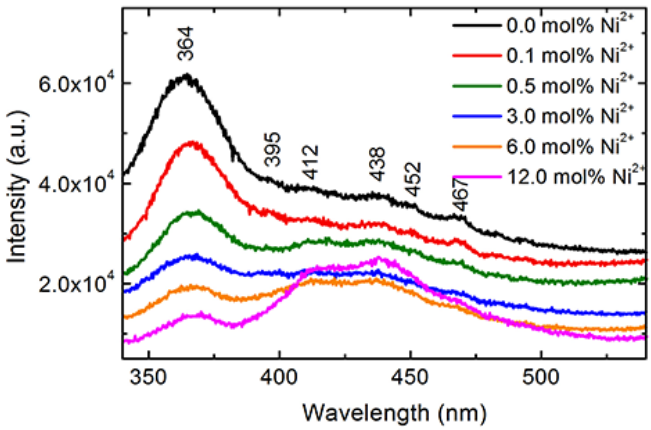

Fig.5. PL emission spectra of the Ni^{2+}-doped SnO_2 samples with different doping concentration.

To find out the effect of Ni^{2+} dopant concentration on the PL properties of the synthesized samples, the PL spectra of the SnO_2 powders doped with 0, 0.1, 0.5, 3.0, 6.0 and 12.0 mol% Ni^{2+} were investigated and are shown in Fig. 5. It can be observed that the intensity of the 364 nm peak decreases when the doping concentration increases. Meanwhile, the intensity of the 412 nm and 438

nm peaks increases with increasing the doping concentration, which are attributed to the increase of oxygen vacancy defects.

4. Conclusion

The SnO_2:Ni^{2+} powders with dopant contents ranging from 0.0 to 12 mol% have been successfully synthesized by sol-gel method. XRD analysis indicated that the synthesized samples with doping concentrations from 0 mol% to 6.0 mol% exhibited single SnO_2 crystalline phase. Above 9.0 mol% Ni-doped concentration, SnO_2:Ni^{2+} exhibited a mixture of SnO_2 and NiO crystalline phases. The lattice parameters of SnO_2 host are independent on Ni^{2+} dopant content, while Raman mode positions are dependent on Ni^{2+} dopant content. Raman spectra measurement shows that there exist the E_g, A_{1g}, B_{2g}, and DA1 modes in all the rutile SnO_2:Ni^{2+} powders and two weak Raman peaks corresponding to TO of A_{2u} mode and structural disorder in the SnO_2 samples doped with 9.0 and 12.0 mol% Ni^{2+}. The PL spectrum of the undoped SnO_2 is characterized by the two emission peaks at 365 nm and 395 nm due to near band edge (NBE) emission; the three shoulders/peaks at 412 nm, 438 nm, 452 nm are the violet emission associated with surface dangling bonds or oxygen vacancies and Sn interstitials; and the peak at 465 nm is due to doubly ionized oxygen vacancies. The Ni^{2+}-doping results in the decrease of the NBE emission, but leades to the increase of the emission related to the oxygen vacancy defects. These results are useful for further studies on optoelectronic materials, for DSSCs in particular.

Acknowledgments

This work is financially supported by VNU Asia Research Center (Project No. CA.18.6A).

References

[1] X. Guan, Y. Wang, P. Luo, Y. Yu, D. Chen, X. Li, Incorporating N Atoms into SnO_2 Nanostructure as an Approach to Enhance Gas Sensing Property for Acetone, Nanomaterials 9 (2019) 1-18. https://doi.org/10.3390/nano9030445.

[2] N.N. Dinh, M.C. Bernard, A.H. Goff, T. Stergiopoulos, P. Falaras, Photoelectrochemical solar cells based on SnO_2 nanocrystalline films, C.R.Chimie 9 (2006) 676-683. https://doi.org/10.1016/j.crci.2005.02.042.

[3] K.K. Sharker, M.A. Khan, S.M.M. Khan, R. Islam, Preparation and Characterization of Tin Oxide based Transparent Conducting Coating for Solar Cell Application**,** Int. J. Thin. Fil. Sci. Tec. 4 (2015) 243-247. http://dx.doi.org/10.12785/ijtfst/040315.

[4] P.K. Mohanta, C. Glökler, A.O. Arenas, L. Jörissen, Sb doped SnO_2 as a stable cathode catalyst support for low temperature polymer electrolyte membrane fuel cell, Int. J. Hydrogen Energy 42 (2017) 27950-27961. http://dx.doi.org/10.1016/j.ijhydene.2017.06.064.

[5] B. Cojocaru, D. Avram, V. Kessler, V. Parvulescu, G. Seisenbaeva, C. Tiseanu, Nanoscale insights into Doping behavior, particle size and surface efects in trivalent metal doped SnO_2, Sci. Rep.-UK 7 (2017) 1-14. https://doi.org/10.1038/s41598-017-09026-2.

[6] A. Die guez, A. Romano-Rodrı guez, A. Vila, J.R. Morante, The complete Raman spectrum of nanometric SnO_2 particles, J. Appl. Phys.90 (2001) 1550-1557. https://doi.org/10.1063/1.1385573.

[7] L. Shi, Y. Xu, Q. Li, Controlled fabrication of SnO_2 arrays of well-aligned nanotubes and nanowires, Nanoscale 2 (2010) 2104–2108. https://doi.org/10.1039/c0nr00279h.

[8] W. Wan, Y. Li, X. Ren, Y. Zhao, F. Gao, H. Zhao, 2D SnO_2 Nanosheets: Synthesis, Characterization, Structures, and Excellent Sensing Performance to Ethylene Glycol, Nanomaterials 8 (2018) 1-20. https://doi.org/10.3390/nano8020112.

[9] X. Wang, X. Wang, Q. Di, H. Zhao, B. Liang and J. Yang, Mutual Effects of Fluorine Dopant and Oxygen Vacancies on Structural and Luminescence Characteristics of F Doped SnO_2, Nanoparticles Materials 10 (2017) 1-12. https://doi.org/10.3390/ma10121398.

[10] Y.M. Lu, J. Jiang, M. Becker, B. Kramm, L. Chen, A. Polity, Y.B. He, P.J. Klar, B.K. Meyer, Polycrystalline SnO_2 films grown by chemical vapor deposition on quartz glass, Vacuum 122B (2015) 347-352. http://dx.doi.org/10.1016/j.vacuum.2015.03.018.

[11] X.S. Peng, L.D. Zhang, G.W. Meng, Y.T. Tian, Y. Lin, Micro-Raman and Infrared properties of Tin Oxide Nanobelts Synthesized from Tin Metal and SiO_2 Powders, J. Appl. Phys. 93 (2003) 1760-1763. https://doi.org/10.1063/1.1534903.

[12] R. Liu, Y. Chen, F. Wang, L. Cao, A. Pan, G. Yang, T. Wang, B. Zou, Stimulated emission from trapped excitons in SnO_2 nanowires, Physica E 39 (2007) 223–229. https://doi.org/10.1016/j.physe.2007.04.009.

[13] N. Salah, S. Habib, A. Azam, M.S. Ansari, W.M. AL-Shawafi, Formation of Mn-doped SnO_2 Nanoparticles Via the Microwave Technique: Structural, Optical and Electrical Properties, Nanomater Nanotechnol 6 (2016) 1-8. https://doi.org/10.5772/62520.

[14] N. Bhardwaj, S. Kuriakose, S. Mohapatra, Structural and optical properties of SnO_2 nanotowers and interconnected nanowires prepared by carbothermal reduction method, J. Alloys Compd. 592 (2014) 238–243. http://dx.doi.org/10.1016/j.jallcom.2013.12.268.

[15] S.H. Luo, Q.Wan, W.L. Liu, M. Zhang, Z.T. Song, C.L. Lin, P.K. Chu, Photoluminescence properties of SnO_2 nanowhiskers grown by thermal evaporation, Prog. Solid State Chem. 33 (2005) 287-292. https://doi.org/10.1016/j.progsolidstchem.2005.11.008.